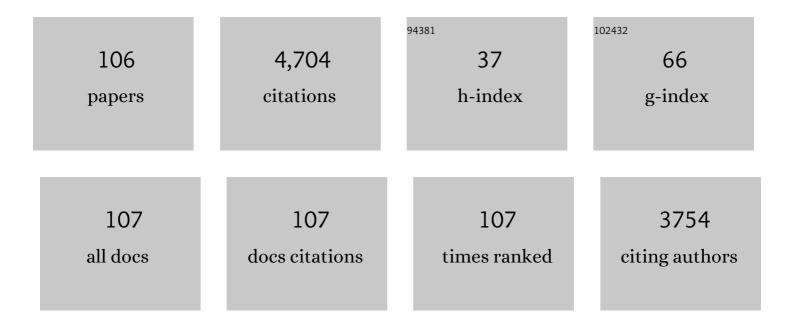
## Hai-Long Zhang

List of Publications by Year in descending order

Source: https://exaly.com/author-pdf/746090/publications.pdf Version: 2024-02-01



#	Article	IF	CITATIONS
1	Compositional Dependence of Piezoelectric Properties in NaxK1-xNbO3 Lead-Free Ceramics Prepared by Spark Plasma Sintering. Journal of the American Ceramic Society, 2006, 89, 1605-1609.	1.9	245
2	Enhanced thermoelectric and mechanical properties in textured n-type Bi2Te3 prepared by spark plasma sintering. Solid State Sciences, 2008, 10, 651-658.	1.5	232
3	Enhanced thermal conductivity in copper matrix composites reinforced with titanium-coated diamond particles. Scripta Materialia, 2011, 65, 1097-1100.	2.6	212
4	Enhanced thermoelectric properties in CoSb3-xTex alloys prepared by mechanical alloying and spark plasma sintering. Journal of Applied Physics, 2007, 102, .	1.1	205
5	A comparative study on Johnson–Cook, modified Johnson–Cook and Arrhenius-type constitutive models to predict the high temperature flow stress in 20CrMo alloy steel. Materials & Design, 2013, 52, 677-685.	5.1	199
6	High thermal conductivity through interfacial layer optimization in diamond particles dispersed Zr-alloyed Cu matrix composites. Scripta Materialia, 2015, 109, 72-75.	2.6	136
7	Compositional dependence of dielectric and ferroelectric properties in BiFeO3–BaTiO3 solid solid solutions. Ceramics International, 2014, 40, 4759-4765.	2.3	122
8	Effects of annealing on electrical properties of n-type Bi2Te3 fabricated by mechanical alloying and spark plasma sintering. Journal of Alloys and Compounds, 2009, 467, 91-97.	2.8	115
9	Phase-transition behavior and piezoelectric properties of lead-free (Ba0.95Ca0.05)(Ti1â^'xZrx)O3 ceramics. Journal of Alloys and Compounds, 2010, 506, 131-135.	2.8	111
10	Effect of Ti interlayer on interfacial thermal conductance between CuÂand diamond. Acta Materialia, 2018, 160, 235-246.	3.8	111
11	Enhanced thermoelectric properties of bismuth sulfide polycrystals prepared by mechanical alloying and spark plasma sintering. Journal of Solid State Chemistry, 2008, 181, 3278-3282.	1.4	103
12	Microstructure and electrical properties of porous PZT ceramics derived from different pore-forming agents. Acta Materialia, 2007, 55, 171-181.	3.8	99
13	Microstructure and thermal conductivity of Cu/diamond composites with Ti-coated diamond particles produced by gas pressure infiltration. Journal of Alloys and Compounds, 2015, 647, 941-946.	2.8	95
14	A bioinspired hybrid membrane with wettability and topology anisotropy for highly efficient fog collection. Journal of Materials Chemistry A, 2019, 7, 124-132.	5.2	93
15	Mechanical and thermal properties of carbon nanotube/aluminum composites consolidated by spark plasma sintering. Materials & Design, 2012, 41, 344-348.	5.1	91
16	Electrical and thermal properties of carbon nanotube bulk materials: Experimental studies for the <mml:math <br="" xmlns:mml="http://www.w3.org/1998/Math/MathML">display="inline"&gt;<mml:mrow><mml:mn>328</mml:mn><mml:mo>â€"</mml:mo><mml:mn>958</mml:mn><mn width="0.3em" /&gt;<mml:mi mathvariant="normal">K</mml:mi></mn </mml:mrow></mml:math> temperature range. Physical Review B, 2007, 75, .	nl:mspace	88
17	Dielectric and piezoelectric properties of (Ba0.95Ca0.05)(Ti0.88Zr0.12)O3 ceramics sintered in a protective atmosphere. Journal of the European Ceramic Society, 2009, 29, 3235-3242.	2.8	88
18	Spark plasma sintering and thermal conductivity of carbon nanotube bulk materials. Journal of Applied Physics, 2005, 97, 114310.	1.1	87

#	Article	IF	CITATIONS
19	Microstructure evolution and impact fracture behaviors of Z3CN20-09M stainless steels after long-term thermal aging. Journal of Nuclear Materials, 2013, 433, 41-49.	1.3	86
20	Optimized thermal properties in diamond particles reinforced copper-titanium matrix composites produced by gas pressure infiltration. Composites Part A: Applied Science and Manufacturing, 2016, 91, 189-194.	3.8	80
21	Enhanced thermal conductivity in Cu/diamond composites by tailoring the thickness of interfacial TiC layer. Composites Part A: Applied Science and Manufacturing, 2018, 113, 76-82.	3.8	80
22	Combining Cr pre-coating and Cr alloying to improve the thermal conductivity of diamond particles reinforced Cu matrix composites. Journal of Alloys and Compounds, 2018, 749, 1098-1105.	2.8	78
23	High thermal conductivity of Cu-B/diamond composites prepared by gas pressure infiltration. Journal of Alloys and Compounds, 2018, 735, 1648-1653.	2.8	75
24	Annealing induced recovery of long-term thermal aging embrittlement in a duplex stainless steel. Materials Science & Engineering A: Structural Materials: Properties, Microstructure and Processing, 2013, 564, 85-91.	2.6	68
25	Thermal conductivity of Cu–Zr/diamond composites produced by high temperature–high pressure method. Composites Part B: Engineering, 2015, 68, 22-26.	5.9	67
26	Microstructures and mechanical properties of cast austenite stainless steels after long-term thermal aging at low temperature. Materials & Design, 2013, 50, 886-892.	5.1	66
27	Tailoring interface structure and enhancing thermal conductivity of Cu/diamond composites by alloying boron to the Cu matrix. Materials Characterization, 2019, 152, 265-275.	1.9	66
28	Effect of copper content on the thermal conductivity and thermal expansion of Al–Cu/diamond composites. Materials & Design, 2012, 39, 87-92.	5.1	65
29	A modified Zerilli–Armstrong constitutive model to predict hot deformation behavior of 20CrMo alloy steel. Materials & Design, 2014, 56, 122-127.	5.1	57
30	A physically-based constitutive model for a nitrogen alloyed ultralow carbon stainless steel. Computational Materials Science, 2015, 98, 64-69.	1.4	56
31	Interfacial structure evolution of Ti-coated diamond particle reinforced Al matrix composite produced by gas pressure infiltration. Composites Part B: Engineering, 2017, 113, 285-290.	5.9	56
32	Interfacial structure evolution and thermal conductivity of Cu-Zr/diamond composites prepared by gas pressure infiltration. Journal of Alloys and Compounds, 2019, 781, 800-809.	2.8	50
33	Nucleation and growth mechanisms of interfacial Al 4 C 3 in Al/diamond composites. Journal of Alloys and Compounds, 2016, 657, 81-89.	2.8	46
34	Grain morphology and crystal structure of pre-transition oxides formed on Zircaloy-4. Corrosion Science, 2013, 74, 323-331.	3.0	44
35	The role of alloying elements in the initiation of nanoscale porosity in oxide films formed on zirconium alloys. Corrosion Science, 2013, 77, 391-396.	3.0	43
36	Precise control of versatile microstructure and properties of graphene aerogel <i>via</i> freezing manipulation. Nanoscale, 2020, 12, 4882-4894.	2.8	43

#	Article	IF	CITATIONS
37	Regulated Interfacial Thermal Conductance between Cu and Diamond by a TiC Interlayer for Thermal Management Applications. ACS Applied Materials & Interfaces, 2019, 11, 26507-26517.	4.0	41
38	Microstructure, Mechanical Properties and InÂVitro Degradation Behavior of a Novel Biodegradable Mg–1.5Zn–0.6Zr–0.2Sc Alloy. Journal of Materials Science and Technology, 2015, 31, 744-750.	5.6	38
39	Effect of metalloid silicon addition on densification, microstructure and thermal–physical properties of Al/diamond composites consolidated by spark plasma sintering. Materials & Design, 2014, 63, 838-847.	5.1	37
40	Mechanical properties of diamond/Al composites with Ti-coated diamond particles produced by gas-assisted pressure infiltration. Materials Science & Engineering A: Structural Materials: Properties, Microstructure and Processing, 2015, 626, 362-368.	2.6	36
41	Interfacial characteristic and thermal conductivity of Al/diamond composites produced by gas pressure infiltration in a nitrogen atmosphere. Materials and Design, 2016, 92, 643-648.	3.3	36
42	Sintering and Piezoelectric Properties of Co-Fired Lead Zirconate Titanate/Ag Composites. Journal of the American Ceramic Society, 2006, 89, 1300-1307.	1.9	35
43	Modified arrhenius-type constitutive model and artificial neural network-based model for constitutive relationship of 316LN stainless steel during hot deformation. Journal of Iron and Steel Research International, 2015, 22, 721-729.	1.4	34
44	Effect of boron addition on interface microstructure and thermal conductivity of Cu/diamond composites produced by high temperature–high pressure method. Physica Status Solidi (A) Applications and Materials Science, 2014, 211, 587-594.	0.8	33
45	The role of Ti coating in enhancing tensile strength of Al/diamond composites. Materials Science & Engineering A: Structural Materials: Properties, Microstructure and Processing, 2013, 565, 33-37.	2.6	32
46	The role of Cr interlayer in determining interfacial thermal conductance between Cu and diamond. Applied Surface Science, 2020, 515, 146046.	3.1	32
47	Preparation and characterization of as-rolled AZ31 magnesium alloy sheets. Journal of Materials Processing Technology, 2007, 184, 102-107.	3.1	31
48	Enhanced thermoelectric property originating from additional carrier pocket in skutterudite compounds. Applied Physics Letters, 2008, 93, .	1.5	31
49	Evolution of copper oxide nanoneedle mesh with subtle regulated lyophobicity for high efficiency liquid separation. Journal of Materials Chemistry A, 2018, 6, 817-822.	5.2	31
50	Enhanced mechanical properties in Ag-particle-dispersed PZT piezoelectric composites for actuator applications. Materials Science & Engineering A: Structural Materials: Properties, Microstructure and Processing, 2008, 498, 272-277.	2.6	29
51	The formation of atomic-level interfacial layer and its effect on thermal conductivity of W-coated diamond particles reinforced Al matrix composites. Composites Part A: Applied Science and Manufacturing, 2018, 107, 164-170.	3.8	29
52	Interfacial products and thermal conductivity of diamond/Al composites reinforced with ZrC-coated diamond particles. Diamond and Related Materials, 2019, 100, 107565.	1.8	28
53	Fabrication and evaluation of PZT/Ag composites and functionally graded piezoelectric actuators. Journal of Electroceramics, 2006, 16, 413-417.	0.8	27
54	Hydrothermal Synthesis of Perovskite <scp><scp>BiFeO<sub>3</sub>–BaTiO<sub>3</sub></scp></scp> Crystallites. Journal of the American Ceramic Society, 2011, 94, 3671-3674.	1.9	27

#	Article	IF	CITATIONS
55	Effect of Metal Matrix Alloying on Mechanical Strength of Diamond Particle-Reinforced Aluminum Composites. Journal of Materials Engineering and Performance, 2015, 24, 2556-2562.	1.2	26
56	Microstructure, mechanical property and inÂvitro biocorrosion behavior of single-phase biodegradable Mg–1.5Zn–0.6Zr alloy. Journal of Magnesium and Alloys, 2014, 2, 181-189.	5.5	25
57	Reinforcement size effect on thermal conductivity in Cu-B/diamond composite. Journal of Materials Science and Technology, 2021, 91, 1-4.	5.6	25
58	Effect of diamond surface chemistry and structure on the interfacial microstructure and properties of Al/diamond composites. RSC Advances, 2016, 6, 67252-67259.	1.7	24
59	Effect of Sintering Temperature on Electrical Properties of Na <sub>0.5</sub> K <sub>0.5</sub> NbO <sub>3</sub> Lead-Free Piezoelectric Ceramics Prepared by Normal Sintering. Ferroelectrics, 2007, 358, 188-195.	0.3	22
60	Morphological healing evolution of penny-shaped fatigue microcracks in pure iron at elevated temperatures. Applied Physics Letters, 2004, 85, 1143-1145.	1.5	21
61	Effect of Zr Content on Mechanical Properties of Diamond/Cu-Zr Composites Produced by Gas Pressure Infiltration. Journal of Materials Engineering and Performance, 2018, 27, 714-720.	1.2	21
62	Reliability enhancement in nickel-particle-dispersed alkaline niobate piezoelectric composites and actuators. Journal of the European Ceramic Society, 2011, 31, 795-800.	2.8	19
63	Electrical and elastic properties of 1–3 PZT/epoxy piezoelectric composites. Journal of Electroceramics, 2008, 21, 410-413.	0.8	17
64	Recrystallization behavior of cold-rolled Zr–1Nb alloy. Journal of Nuclear Materials, 2015, 456, 321-328.	1.3	17
65	Mo-interlayer-mediated thermal conductance at Cu/diamond interface measured by time-domain thermoreflectance. Composites Part A: Applied Science and Manufacturing, 2020, 135, 105921.	3.8	17
66	Unveiling interfacial structure and improving thermal conductivity of Cu/diamond composites reinforced with Zr-coated diamond particles. Vacuum, 2022, 202, 111133.	1.6	17
67	Probabilistic fracture mechanics analysis of thermally aged nuclear piping in a pressurized water reactor. Nuclear Engineering and Design, 2013, 265, 611-618.	0.8	16
68	Tunable coefficient of thermal expansion of Cu-B/diamond composites prepared by gas pressure infiltration. Journal of Alloys and Compounds, 2019, 794, 473-481.	2.8	16
69	Diffusive healing of intergranular fatigue microcracks in iron during annealing. Materials Science & Engineering A: Structural Materials: Properties, Microstructure and Processing, 2004, 382, 171-180.	2.6	15
70	Effects of prior solution treatment on thermal aging behavior of duplex stainless steels. Journal of Nuclear Materials, 2013, 441, 337-342.	1.3	15
71	Tensile behaviour of 316LN stainless steel at elevated temperatures. Materials at High Temperatures, 2014, 31, 198-203.	0.5	15
72	Microstructure and thermal conductivity of AlN coating on Cu substrate deposited by arc ion plating. Materials Chemistry and Physics, 2020, 241, 122374.	2.0	15

#	Article	IF	CITATIONS
73	Covalently Silane-Functionalized Antimonene Nanosheets and Their Copolymerized Gel Glasses for Broadband Vis–NIR Optical Limiting. ACS Applied Materials & Interfaces, 2021, 13, 897-903.	4.0	15
74	Aluminum carbide hydrolysis induced degradation of thermal conductivity and tensile strength in diamond/aluminum composite. Journal of Composite Materials, 2018, 52, 2709-2717.	1.2	14
75	Interface characterization of a Cu–Ti-coated diamond system. Surface and Coatings Technology, 2015, 278, 163-170.	2.2	13
76	Study of Static Recrystallization Behavior of a Nitrogen-Alloyed Ultralow Carbon Austenitic Stainless Steel by Experiment and Simulation. Journal of Materials Engineering and Performance, 2015, 24, 4346-4357.	1.2	12
77	Sintering and electrical properties of Cu-particle-dispersed (Na,K,Li)NbO3. Ceramics International, 2010, 36, 583-587.	2.3	11
78	Calculation of Jackson's factor of Mg2Si in Mg melt using coordination polyhedron. Journal of Alloys and Compounds, 2013, 581, 494-497.	2.8	11
79	High-Temperature Thermal Conductivity and Thermal Cycling Behavior of Cu–B/Diamond Composites. IEEE Transactions on Components, Packaging and Manufacturing Technology, 2020, 10, 626-636.	1.4	11
80	Electrical properties of Ni-particle-dispersed alkaline niobate composites sintered in a protective atmosphere. Materials Chemistry and Physics, 2010, 122, 237-240.	2.0	10
81	Effect of thermal aging on the fatigue crack growth behavior of cast duplex stainless steels. International Journal of Minerals, Metallurgy and Materials, 2015, 22, 1163-1170.	2.4	9
82	Enhanced mechanical properties in Al/diamond composites by Si addition. Rare Metals, 2016, 35, 701-704.	3.6	8
83	Microstructural evolution of sandwiched Cr interlayer in Cu/Cr/diamond subjected to heat treatment. Thin Solid Films, 2021, 736, 138911.	0.8	8
84	Effect of Li content on the microstructure and properties of lead-free piezoelectric (K0.5Na0.5)1–xLixNbO3 ceramics prepared by SPS. International Journal of Minerals, Metallurgy, and Materials, 2008, 15, 314-319.	0.2	7
85	Effect of yttrium addition on microstructure and orientation of hydride precipitation in Zr-1Nb alloy. International Journal of Hydrogen Energy, 2014, 39, 21116-21126.	3.8	7
86	Effect of thermal aging on the leak-before-break analysis of nuclear primary pipes. Nuclear Engineering and Design, 2014, 280, 493-500.	0.8	7
87	Influence of Initial Microstructures on Deformation Behavior of 316LN Austenitic Steels at 400-900°C. Journal of Materials Engineering and Performance, 2015, 24, 694-699.	1.2	7
88	Uniaxial compressive stress and temperature dependent mechanical behavior of (1- x )BiFeO 3 - x BaTiO 3 lead-free piezoelectric ceramics. Ceramics International, 2017, 43, 9092-9098.	2.3	7
89	Mechanical Properties of Cu-B/Diamond Composites Prepared by Gas Pressure Infiltration. Journal of Materials Engineering and Performance, 2020, 29, 3107-3119.	1.2	7
90	Cu-particle-dispersed (K0.5Na0.5)NbO3 composite thin films derived from sol–gel processing. Journal of Sol-Gel Science and Technology, 2012, 61, 403-410.	1.1	6

#	Article	IF	CITATIONS
91	Effects of thermal aging temperature and Cr content on phase separation kinetics in Fe-Cr alloys simulated by the phase field method. International Journal of Minerals, Metallurgy and Materials, 2013, 20, 1067-1075.	2.4	6
92	Flow Behavior Modeling of a Nitrogen-Alloyed Ultralow Carbon Stainless Steel During Hot Deformation: A Comparative Study of Constitutive Models. Journal of Materials Engineering and Performance, 2015, 24, 4106-4118.	1.2	6
93	Characterization of Impact Deformation Behavior of a Thermally Aged Duplex Stainless Steel by EBSD. Acta Metallurgica Sinica (English Letters), 2018, 31, 798-806.	1.5	6
94	Morphological healing evolution of intragranular penny-shaped microcracks by surface diffusion: Part II. Experiments. Metallurgical and Materials Transactions A: Physical Metallurgy and Materials Science, 2003, 34, 287-294.	1.1	5
95	Corrosion behavior of Zr–Nb–Cr cladding alloys. Rare Metals, 2013, 32, 480-485.	3.6	4
96	Finite element analysis and experimental study of microstructure evolution of nitrogen alloyed ultralow carbon stainless steel during hot deformation. Materials at High Temperatures, 2015, 32, 502-511.	0.5	4
97	A physically based dynamic recrystallization model considering orientation effects for a nitrogen alloyed ultralow carbon stainless steel during hot forging. Journal of Iron and Steel Research International, 2016, 23, 364-371.	1.4	4
98	Leak-before-break analysis of thermally aged nuclear pipe under different bending moments. Nuclear Engineering and Technology, 2015, 47, 712-718.	1.1	3
99	Characterization of Plastic Deformation Behavior of a Thermally Aged Duplex Stainless Steel. Journal of Materials Engineering and Performance, 2017, 26, 2814-2825.	1.2	3
100	Electrical properties tailoring in Ni-particle-dispersed (Ba0.95Ca0.05)(Ti0.96Zr0.04)O3 composites. Materials Chemistry and Physics, 2011, 126, 729-733.	2.0	2
101	Density changes of iron during morphological healing evolution of internal fatigue microcracks. Metallurgical and Materials Transactions A: Physical Metallurgy and Materials Science, 2003, 34, 2925-2933.	1.1	1
102	A Method to Prepare TEM Specimens by Focused Ion Beam Milling for Cu/diamond Composites. Microscopy and Microanalysis, 2018, 24, 838-839.	0.2	1
103	THERMAL CONDUCTIVITY AND THERMAL AGING PERFORMANCE OF Sn WITH 0.7 wt.% Cu and VARIOUS GRAPHENE ADDITIONS. Surface Review and Letters, 2020, 27, 1950161.	0.5	1
104	Hot Tensile Deformation and Fracture Behavior of a Nitrogen Alloyed Ultralow Carbon Austenitic Stainless Steel. Materials Transactions, 2015, 56, 1984-1991.	0.4	0
105	Interface tailoring and thermal conductivity enhancement in diamond particles reinforced metal matrix composites. , 2020, , 473-493.		0
106	Study on LBB Behavior of Nuclear Primary Pipes After Long-Term Thermal Aging. , 2014, , 501-508.		0